Supplementary information

Fe^{2+}/Fe^{3+} -Mediated Synergistic Electrochemical Leaching of Spent Lithium-Ion Batteries under Low Voltage: A Green Chemistry Approach

Kenan Zhong[a], Mengjia Kang[a], Zhuo Ye[a], Bicheng Meng[a], Xueyang Hou[a], Zhongliang Tian[b], Kai Yang[a, *], Qingjuan Wang [a, *], Zhao Fang[a, c *],

[a] School of Metallurgical Engineering, Xi'an University of Architecture and Technology, Xi'an, 710055, China.

[b] School of Metallurgy and Environment, Central South University, Changsha, 410083, China.

[c] Shaanxi Engineering Research Center of Metallurgical, Xi'an, China

***Corresponding Authors**

E-mail address: yangkaiyj@xauat.edu.cn (K. Yang)

E-mail address: jiandawqj@163.com (Q. Wang)

E-mail address: fangzhao@xauat.edu.cn (Z. Fang)

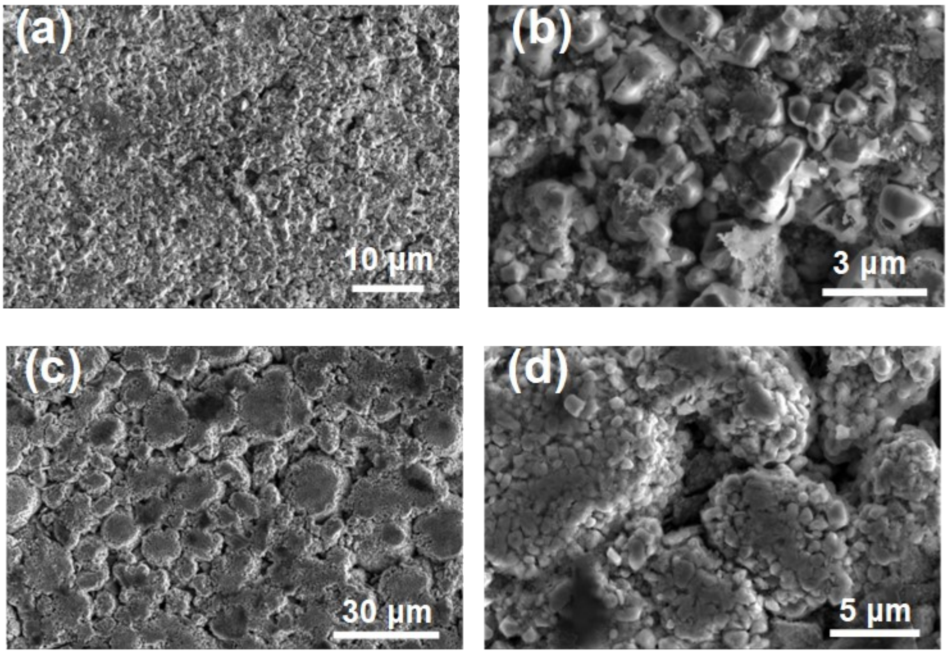

Figure S1 The SEM images of spent (a-b) LFP and (b) NCM cathode plate.

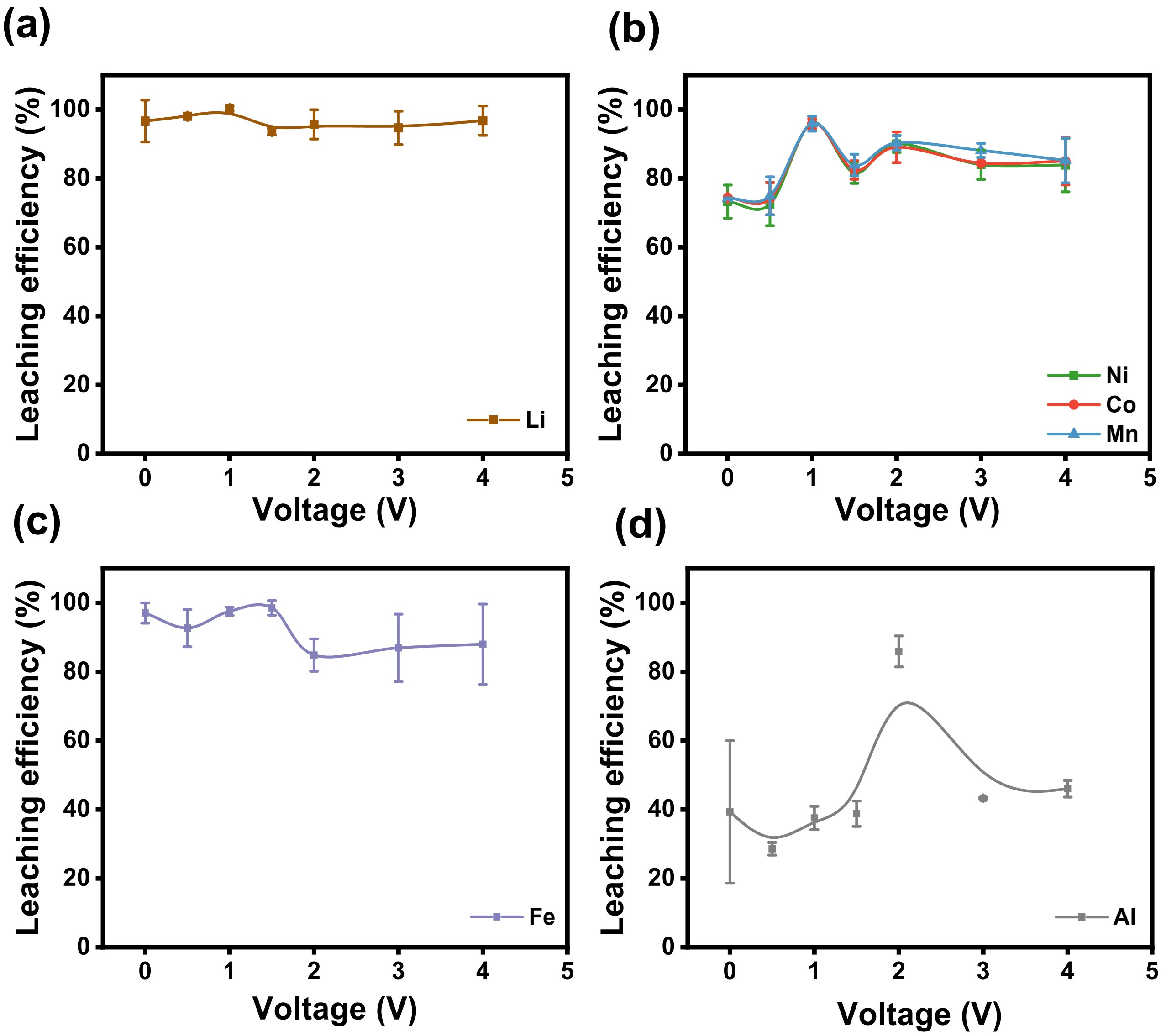

Figure S2 Leaching efficiency of each element at different voltages after 120min leaching at 50 °C, 1M H_2SO_4 concentration.

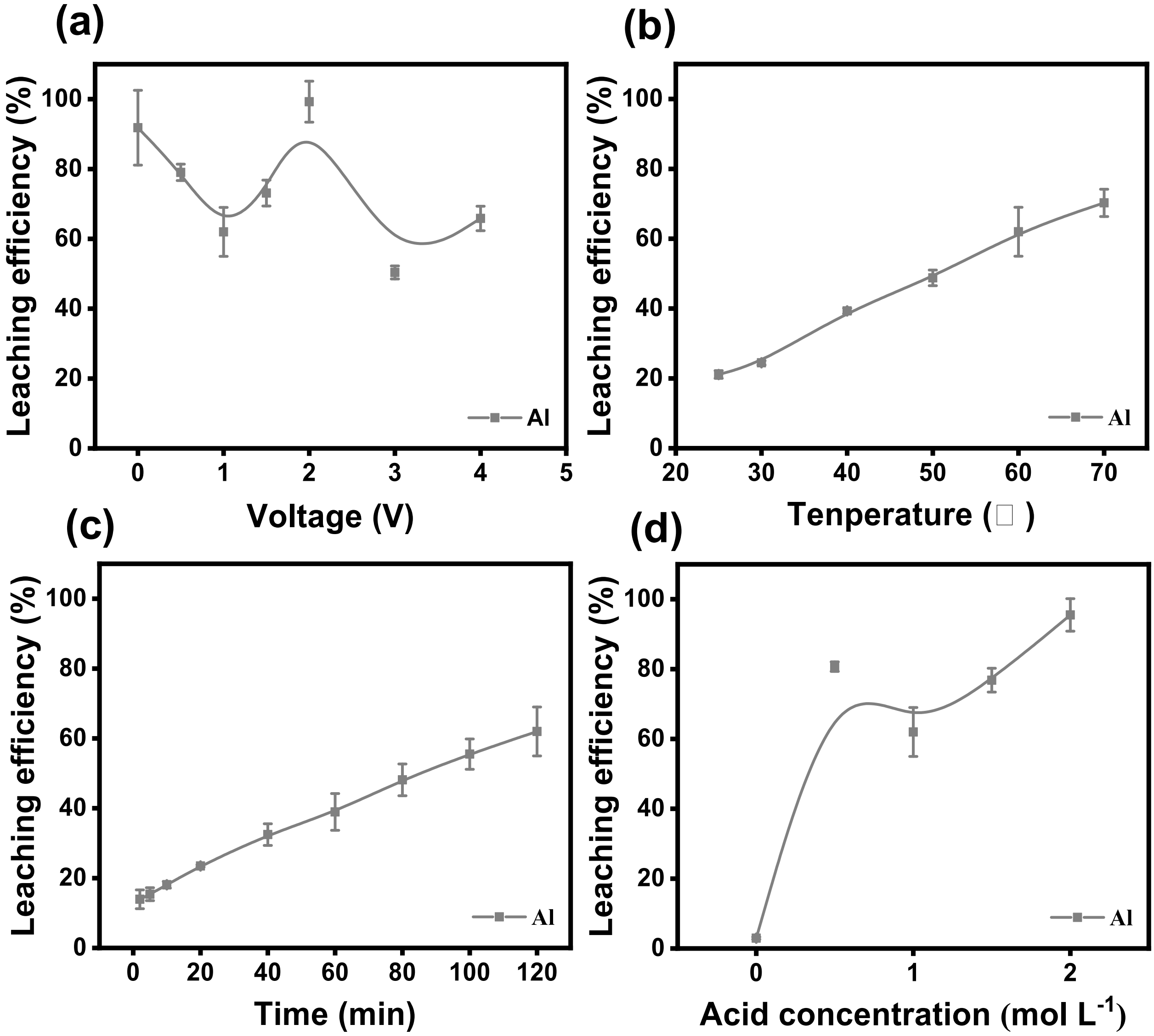

Figure S3. Different (a)voltage, (b)reaction temperature, (c)leaching time, (d)H_2SO_4 concentration effects on Al leaching efficiency.

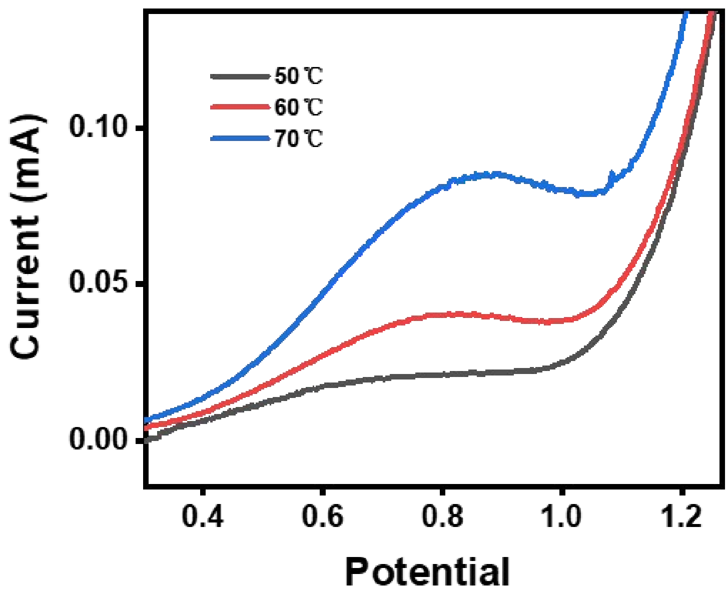

Figure S4 The LSV curves of two electrodes, with Pt as both the cathode and anode in a 1M H_2SO_4 solution at different temperatures by 10 mV s^{-1}.

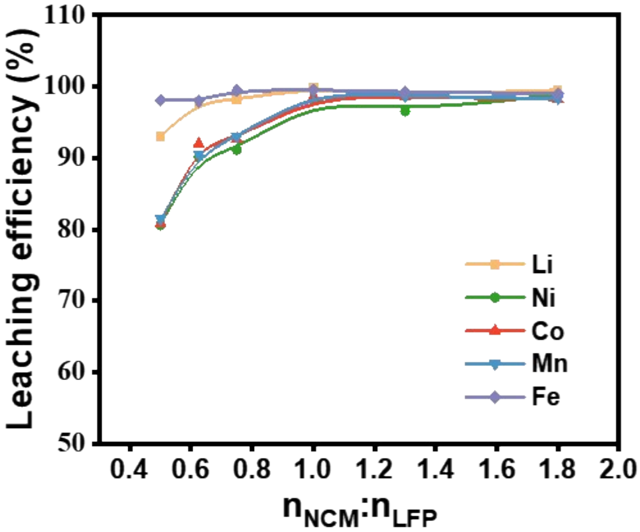

Figure S5 Leaching efficiency of NCM and LFP under different active material ratios of electrolytic cathode and anode (n_{LFP}:n_{NCM}).

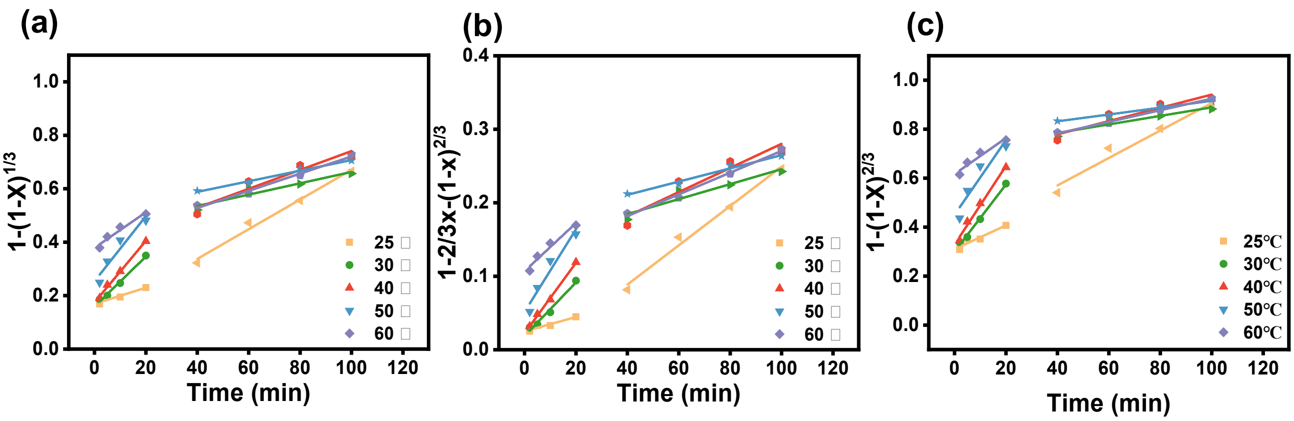

Figure S6. Plots of (a) *1-(1-x)*$^{1/3}$ vs. *t*, (b) *1-2/3x-(1-x)*$^{2/3}$ *vs*. *t* and (c) *1-(1-x)*$^{2/3}$ *vs*. *t* at different reaction temperatures for Li.

Table S1. Fitting results of kinetic models of Li under different temperature parameters (*(1-(1-x)$^{1/3}$* vs. *t*, *1-2/3x-(1-x)$^{2/3}$* vs. *t* and *1-(1-x)$^{2/3}$* vs. *t*.

Element	Temperature (℃)	Kinetic Equation	Time (min)	Fit Equation	R^2
Li	25	$1-(1-x)^{1/3}$	2-20	y=0.003029x+0.169175	0.901858
			40-100	y=0.005554x+0.115333	0.986228
		$1-2/3x-(1-x)^{2/3}$	2-20	y=0.000976x+0.025033	0.91257
			40-100	y=0.002675x-0.018401	0.987627
		$1-(1-x)^{2/3}$	2-20	y=0.004833x+0.310326	0.897694
			40-100	y=0.005605x+0.346080	0.956515
	30	$1-(1-x)^{1/3}$	2-20	y=0.009374x+0.158900	0.990798
			40-100	y=0.002122x+0.450668	0.917719
		$1-2/3x-(1-x)^{2/3}$	2-20	y=0.003647x+0.018676	0.981259
			40-100	y=0.001020x+0.143744	0.910686
		$1-(1-x)^{2/3}$	2-20	y=0.013702x+0.300007	0.994076
			40-100	y=0.001741x+0.715011	0.89415
	40	$1-(1-x)^{1/3}$	2-20	y=0.011530x+0.174657	0.99572
			40-100	y=0.002345x+0.439882	0.889967
		$1-2/3x-(1-x)^{2/3}$	2-20	y=0.004792x+0.022520	0.997909
			40-100	y=0.001098x+0.140034	0.875845
		$1-(1-x)^{2/3}$	2-20	y=0.016068x+0.328619	0.989642
			40-100	y=0.002707x+0.670575	0.848844
	50	$1-(1-x)^{1/3}$	2-20	y=0.001819x+0.710739	0.923326
			40-100	y=0.002659x+0.472905	0.960189
		$1-2/3x-(1-x)^{2/3}$	2-20	y=0.005613x+0.051640	0.942304
			40-100	y=0.001168x+0.160498	0.970563
		$1-(1-x)^{2/3}$	2-20	y=0.015250x+0.450204	0.89287
			40-100	y=0.001763x+0.756660	0.979153
	60	$1-(1-x)^{1/3}$	2-20	y=0.006650x+0.378904	0.953651
			40-100	y=0.003214x+0.399408	0.984421
		$1-2/3x-(1-x)^{2/3}$	2-20	y=0.003272x+0.107002	0.957499
			40-100	y=0.001478x+0.122737	0.99031
		$1-(1-x)^{2/3}$	2-20	y=0.007352x+0.616699	0.937703
			40-100	y=0.002370x+0.687805	0.995975

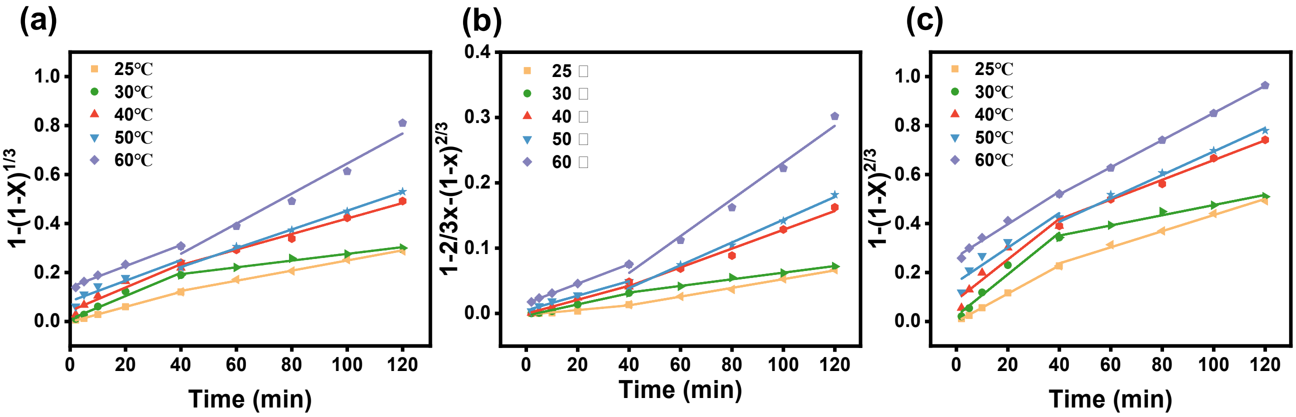

Figure S7. Plots of (a) $1-(1-x)^{1/3}$ vs. t, (b) $1-2/3x-(1-x)^{2/3}$ *vs*. t and (c) $1-(1-x)^{2/3}$ *vs*. t at different reaction temperatures for Ni.

Table S2. Fitting results of kinetic models of Ni under different temperature parameters ($(1-(1-x)^{1/3}$ vs. t, $1-2/3x-(1-x)^{2/3}$ vs. t and $1-(1-x)^{2/3}$ vs. t.

Element	Temperature (℃)	Kinetic Equation	Time (min)	Fit Equation	R^2
Ni	25	$1-(1-x)^{1/3}$	2-20	y=0.003064x-0.001656	0.999565
			40-100	y=0.002072x+0.041855	0.996521
		$1-2/3x-(1-x)^{2/3}$	2-20	y=0.000361x-0.001978	0.949231
			40-100	y=0.000669x-0.014353	0.995311
		$1-(1-x)^{2/3}$	2-20	y=0.005736x-0.001120	0.999356
			40-100	y=0.003292x+0.105371	0.993057
	30	$1-(1-x)^{1/3}$	2-20	y=0.004734x+0.009293	0.974564
			40-100	y=0.001378x+0.138313	0.985113
		$1-2/3x-(1-x)^{2/3}$	2-20	y=0.000854x-0.003241	0.991449
			40-100	y=0.000508x+0.011708	0.991607
		$1-(1-x)^{2/3}$	2-20	y=0.011680x-0.002122	0.999285
			40-100	y=0.002080x+0.267377	0.980650
	40	$1-(1-x)^{1/3}$	2-20	y=0.004773x+0.043187	0.984156
			40-100	y=0.003380x+0.082414	0.993712
		$1-2/3x-(1-x)^{2/3}$	2-20	y=0.001069x-0.000399	0.988762
			40-100	y=0.001514x-0.023251	0.983828
		$1-(1-x)^{2/3}$	2-20	y=0.007066x+0.160018	0.894065
			40-100	y=0.004354x+0.223563	0.994276
	50	$1-(1-x)^{1/3}$	2-20	y=0.004207x+0.082259	0.974875
			40-100	y=0.003622x+0.090065	0.997914
		$1-2/3x-(1-x)^{2/3}$	2-20	y=0.001114x+0.004906	0.980803
			40-100	y=0.001669x-0.023392	0.992143
		$1-(1-x)^{2/3}$	2-20	0.007066x+0.160018	0.894065
			40-100	y=0.004464x+0.247686	0.999332
	60	$1-(1-x)^{1/3}$	2-20	y=0.004309x+0.139886	0.989375
			40-100	y=0.006926x-0.047525	0.975262
		$1-2/3x-(1-x)^{2/3}$	2-20	y=0.001498x+0.015606	0.999144
			40-100	y=0.003146x-0.083567	0.988718
		$1-(1-x)^{2/3}$	2-20	y=0.006654x+0.263927	0.982099
			40-100	y=0.005603x+0.291143	0.999938

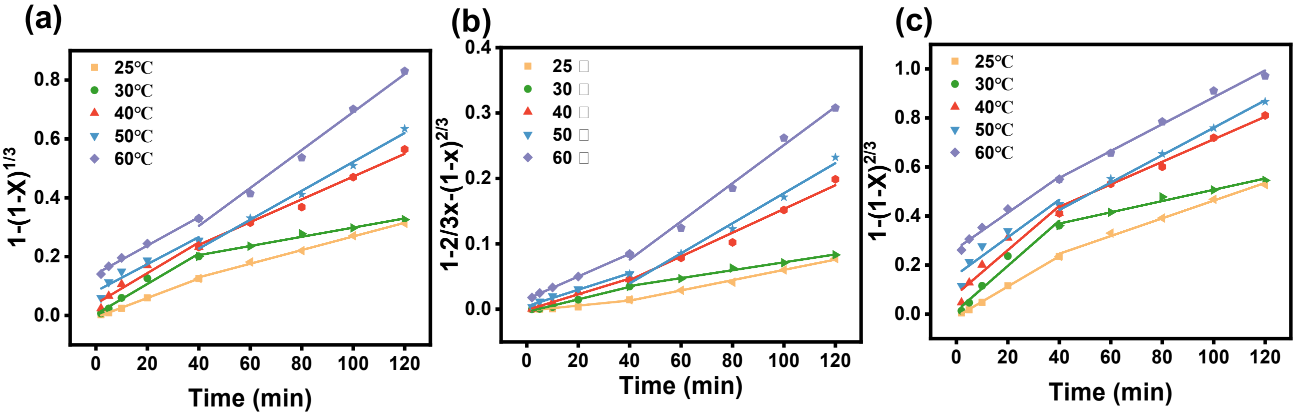

Figure S8. Plots of (a) $1\text{-}(1\text{-}x)^{1/3}$ vs. t, (b) $1\text{-}2/3x\text{-}(1\text{-}x)^{2/3}$ *vs*. t and (c) $1\text{-}(1\text{-}x)^{2/3}$ *vs*. t at different reaction temperatures for Co.

Table S3. . Fitting results of kinetic models of Co under different temperature parameters (*(1-(1-x)*$^{1/3}$ vs. *t*, *1-2/3x-(1-x)*$^{2/3}$ vs. *t* and *1-(1-x)*$^{2/3}$ vs. *t*.

Element	Temperature (°C)	Kinetic Equation	Time (min)	Fit Equation	R^2
Co	25	$1-(1-x)^{1/3}$	2-20	y=0.003236x-0.006190	0.994592
			40-100	y=0.002318x+0.036786	0.997133
		$1-2/3x-(1-x)^{2/3}$	2-20	y=0.000197x-0.000801	0.923095
			40-100	y=0.000821x-0.021887	0.993105
		$1-(1-x)^{2/3}$	2-20	y=0.006172x-0.010807	0.999021
			40-100	y=0.003613x+0.101684	0.993575
	30	$1-(1-x)^{1/3}$	2-20	y=0.006708x-0.008074	0.999255
			40-100	y=0.001562x+0.142366	0.985717
		$1-2/3x-(1-x)^{2/3}$	2-20	y=0.000839x-0.003118	0.950558
			40-100	y=0.000586x+0.013111	0.984181
		$1-(1-x)^{2/3}$	2-20	y=0.009204x+0.012792	0.969043
			40-100	y=0.002300x+0.277220	0.980737
	40	$1-(1-x)^{1/3}$	2-20	y=0.005213x+0.039487	0.933339
			40-100	y=0.004095x+0.062431	0.989844
		$1-2/3x-(1-x)^{2/3}$	2-20	y=0.001201x-0.001193	0.992394
			40-100	y=0.001897x-0.036410	0.981578
		$1-(1-x)^{2/3}$	2-20	y=0.008998x+0.081139	0.915567
			40-100	y=0.004936x+0.219531	0.994850
	50	$1-(1-x)^{1/3}$	2-20	y=0.004604x+0.082075	0.916518
			40-100	y=0.004688x+0.053041	0.988484
		$1-2/3x-(1-x)^{2/3}$	2-20	y=0.001261x+0.004597	0.983447
			40-100	y=0.002214x-0.043989	0.981977
		$1-(1-x)^{2/3}$	2-20	y=0.005324x+0.232478	0.999968
			40-100	y=0.005251x+0.235086	0.999897
	60	$1-(1-x)^{1/3}$	2-20	y=0.004821x+0.141046	0.990317
			40-100	y=0.007069x-0.015689	0.996785
		$1-2/3x-(1-x)^{2/3}$	2-20	y=0.001732x+0.015413	0.999365
			40-100	y=0.003140x-0.062992	0.991596
		$1-(1-x)^{2/3}$	2-20	y=0.007331x+0.266906	0.982280
			40-100	y=0.005346x+0.349760	0.977017

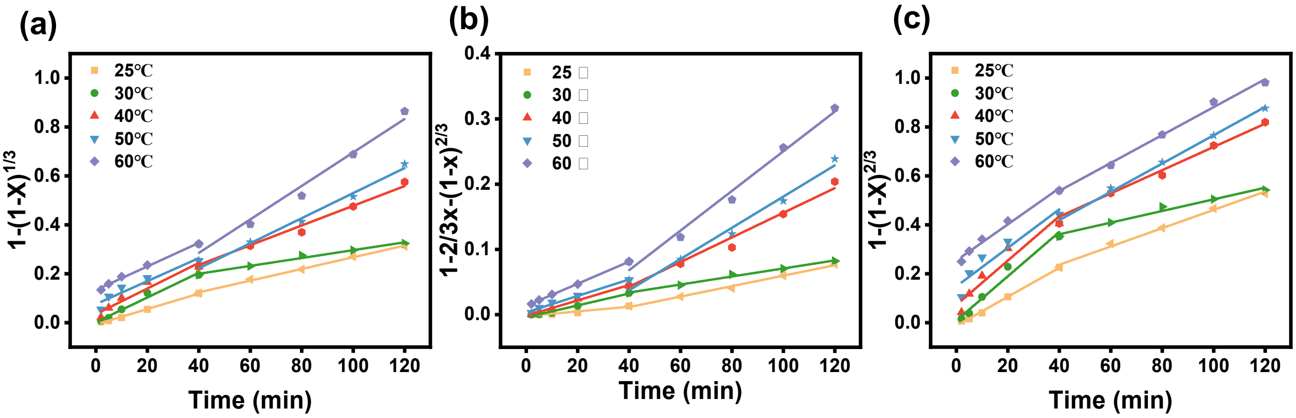

Figure S9. Plots of (a) $1\text{-}(1\text{-}x)^{1/3}$ vs. t, (b) $1\text{-}2/3x\text{-}(1\text{-}x)^{2/3}$ *vs*. t and (c) $1\text{-}(1\text{-}x)^{2/3}$ *vs*. t at different reaction temperatures for Mn .

Table S4. Fitting results of kinetic models of Mn under different temperature parameters (*(1-(1-x)^{1/3}* vs. *t*, *1-2/3x-(1-x)^{2/3}* vs. *t* and *1-(1-x)^{2/3}* vs. *t*.

Element	Temperature (℃)	Kinetic Equation	Time (min)	Fit Equation	R2
Mn	25	$1-(1-x)^{1/3}$	2-20	y=0.003153x-0.007435	0.995886
			40-100	y=0.002389x+0.028400	0.997304
		$1-2/3x-(1-x)^{2/3}$	2-20	y=0.000357x-0.002185	0.928030
			40-100	y=0.000843x-0.024498	0.993268
		$1-(1-x)^{2/3}$	2-20	y=0.005917x-0.012466	0.996973
			40-100	y=0.003737x+0.087319	0.993694
	30	$1-(1-x)^{1/3}$	2-20	y=0.005050x+0.001835	0.979449
			40-100	y=0.001609x+0.135566	0.984766
		$1-2/3x-(1-x)^{2/3}$	2-20	y=0.000910x-0.004017	0.985838
			40-100	y=0.000597x+0.011166	0.984301
		$1-(1-x)^{2/3}$	2-20	y=0.009056x+0.008505	0.971899
			40-100	y=0.002380x+0.266193	0.979321
	40	$1-(1-x)^{1/3}$	2-20	y=0.005230x+0.034951	0.938156
			40-100	y=0.004267x+0.051099	0.989469
		$1-2/3x-(1-x)^{2/3}$	2-20	y=0.001177x-0.001667	0.993287
			40-100	y=0.001977x-0.041456	0.980697
		$1-(1-x)^{2/3}$	2-20	y=0.009065x+0.072544	0.921393
			40-100	y=0.005116x+0.206932	0.995222
	50	$1-(1-x)^{1/3}$	2-20	y=0.004708x+0.075570	0.922387
			40-100	y=0.004889x+0.040777	0.986632
		$1-2/3x-(1-x)^{2/3}$	2-20	y=0.001263x+0.003461	0.987675
			40-100	y=0.002305x-0.049478	0.980088
		$1-(1-x)^{2/3}$	2-20	y=0.005465x+0.222555	0.999988
			40-100	y=0.005423x+0.223989	0.999914
	60	$1-(1-x)^{1/3}$	2-20	y=0.004816x+0.133543	0.991949
			40-100	y=0.007769x-0.080984	0.991643
		$1-2/3x-(1-x)^{2/3}$	2-20	y=0.001694x+0.013527	0.999518
			40-100	y=0.003370x-0.086565	0.995986
		$1-(1-x)^{2/3}$	2-20	y=0.007393x+0.254022	0.984692
			40-100	y=0.005748x+0.306425	0.989013

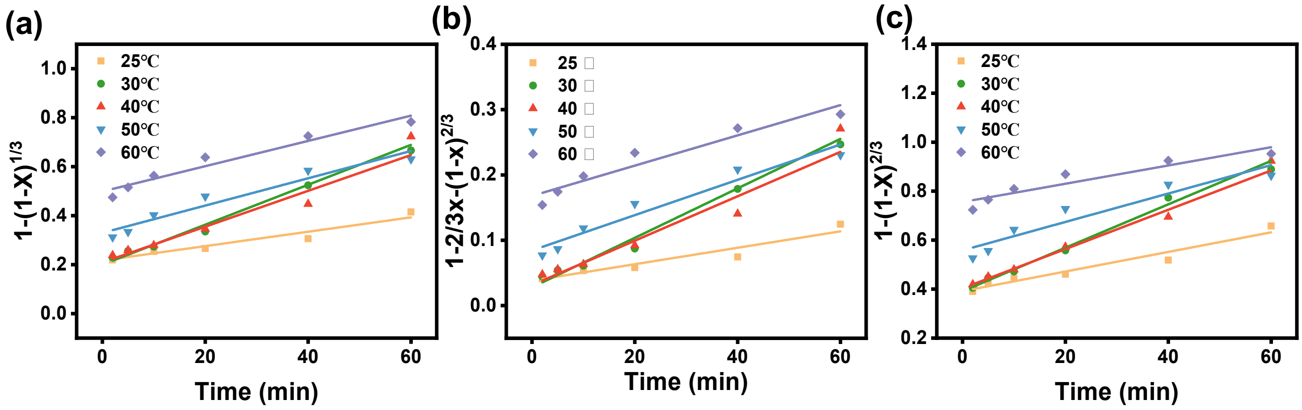

Figure S10. Plots of (a) $1-(1-x)^{1/3}$ vs. t, (b) $1-2/3x-(1-x)^{2/3}$ *vs*. t and (c) $1-(1-x)^{2/3}$ *vs*. t at different reaction temperatures for Fe .

Table S5. Fitting results of kinetic models of Fe under different temperature parameters (*(1-(1-x)$^{1/3}$* vs. *t*, *1-2/3x-(1-x)$^{2/3}$* vs. *t* and *1-(1-x)$^{2/3}$* vs. *t*.

Element	Temperature (℃)	Kinetic Equation	Time (min)	Fit Equation	R2
Fe	25	$1-(1-x)^{1/3}$	2-60	y=0.002936t+0.216871	0.906618
		$1-2/3x-(1-x)^{2/3}$	2-60	y=0.001258t+0.038199	0.892645
		$1-(1-x)^{2/3}$	2-60	y=0.004003t+0.391695	0.916016
	30	$1-(1-x)^{1/3}$	2-60	y=0.008156t+0.199791	0.992360
		$1-2/3x-(1-x)^{2/3}$	2-60	y=0.003787t+0.027949	0.987807
		$1-(1-x)^{2/3}$	2-60	y=0.008866t+0.391534	0.994003
	40	$1-(1-x)^{1/3}$	2-60	y=0.006534x+0.217399	0.986010
		$1-2/3x-(1-x)^{2/3}$	2-60	y=0.001341x+0.002597	0.994122
		$1-(1-x)^{2/3}$	2-60	y=0.006865x+0.159697	0.939148
	50	$1-(1-x)^{1/3}$	2-60	y=0.006355x+0.320875	0.977305
		$1-2/3x-(1-x)^{2/3}$	2-60	y=0.003055x+0.080490	0.978169
		$1-(1-x)^{2/3}$	2-60	y=0.006338x+0.552193	0.938657
	60	$1-(1-x)^{1/3}$	2-60	y=0.005160t+0.498734	0.947854
		$1-2/3x-(1-x)^{2/3}$	2-60	y=0.002317t+0.167936	0.925249
		$1-(1-x)^{2/3}$	2-60	y=0.003731t+0.755601	0.889661

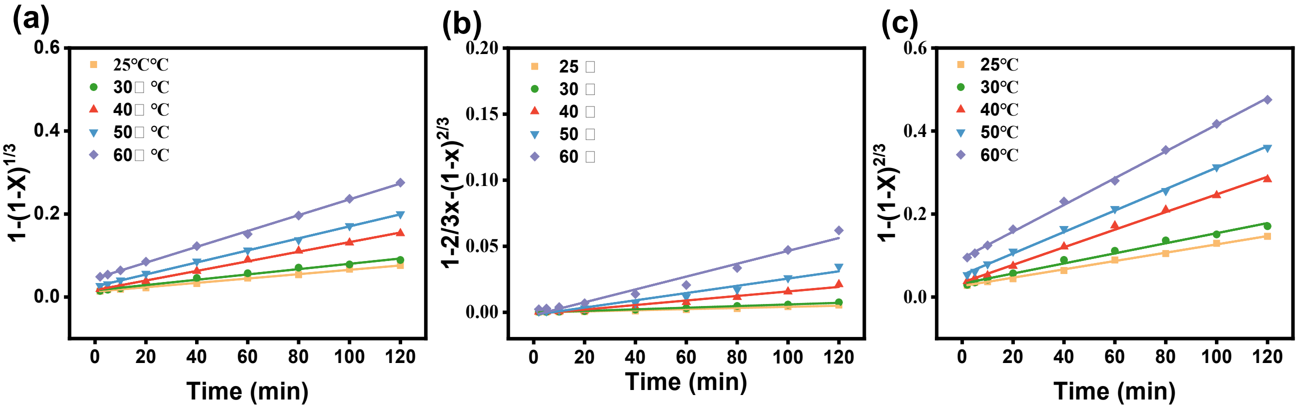

Figure S11. Plots of (a) $1\text{-}(1\text{-}x)^{1/3}$ vs. t, (b) $1\text{-}2/3x\text{-}(1\text{-}x)^{2/3}$ *vs*. t and (c) $1\text{-}(1\text{-}x)^{2/3}$ *vs*. t at different reaction temperatures for Al.

Table S6. Fitting results of kinetic models of Al under different temperature parameters (*(1-(1-x)$^{1/3}$* vs. *t*, *1-2/3x-(1-x)$^{2/3}$* vs. *t* and *1-(1-x)$^{2/3}$* vs. *t*.

Element	Temperature (℃)	Kinetic Equation	Time (min)	Fit Equation	R2
		$1-(1-x)^{1/3}$	2-120	y=0.000524x+0.013212	0.996689
	25	$1-2/3x-(1-x)^{2/3}$	2-120	y=0.000043x-0.000223	0.962664
		$1-(1-x)^{2/3}$	2-120	y=0.001002x+0.026678	0.996901
		$1-(1-x)^{1/3}$	2-120	y=0.000640x+0.016075	0.990023
	30	$1-2/3x-(1-x)^{2/3}$	2-120	y=0.000061x-0.000194	0.992448
		$1-(1-x)^{2/3}$	2-120	y=0.001215x+0.032389	0.988111
		$1-(1-x)^{1/3}$	2-120	y=0.001156x+0.016694	0.998331
Al	40	$1-2/3x-(1-x)^{2/3}$	2-120	y=0.000172x-0.001363	0.972853
		$1-(1-x)^{2/3}$	2-120	y=0.002122x+0.035023	0.997056
		$1-(1-x)^{1/3}$	2-120	y=0.001449x+0.025404	0.999002
	50	$1-2/3x-(1-x)^{2/3}$	2-120	y=0.000275x-0.001911	0.965009
		$1-(1-x)^{2/3}$	2-120	y=0.002584x+0.053318	0.998228
		$1-(1-x)^{1/3}$	2-120	y=0.001906x+0.044754	0.998714
	60	$1-2/3x-(1-x)^{2/3}$	2-120	y=0.000487x-0.002165	0.968577
		$1-(1-x)^{2/3}$	2-120	y=0.003221x+0.093172	0.998678

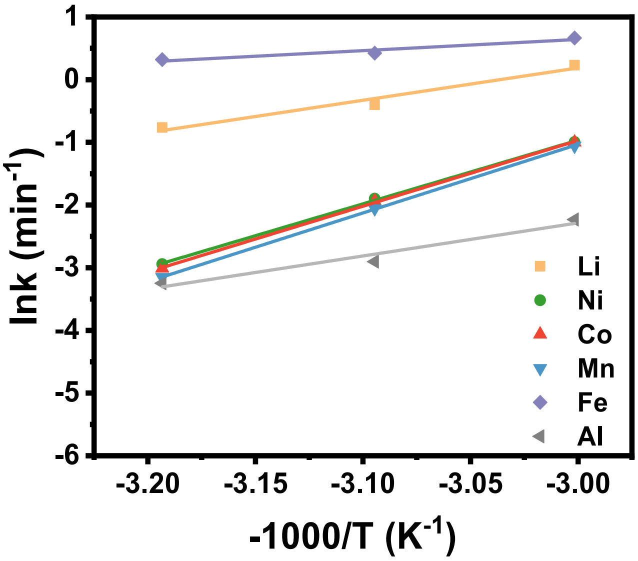

Fig.S12. linear fitting of *lnk* vs *-1000/T* for leaching of Li, Ni, Co, Mn, Fe and Al.

Table S7 Kinetic parameters of Li, Ni, Co, Mn and Fe in the Avrami equation at different leaching temperatures.

Element	Temperature (°C)	Time (min)	n	lnk	R^2
Li	25	2-20	0.13650	-0.682411	0.896659
		40-100	1.100022	-3.890266	0.993923
	30	2-20	0.315255	0.796898	0.872429
		40-100	0.390078	-0.627451	0.960119
	40	2-20	0.377676	-0.762456	0.965990
		40-100	0.654135	-1.636778	0.977655
	50	2-20	0.363201	0.401380	0.999033
		40-100	0.460440	0.757091	0.888284
	60	2-40	0.167955	0.231405	0.993050
		40-100	0.561406	-1.276100	0.934297
Ni	25	2-40	1.052755	-4.859077	0.996551
		40-120	0.875089	-4.175156	0.997990
	30	2-40	1.022669	-4.108887	0.993256
		40-120	0.484873	-2.257159	0.995040
	40	2-40	0.792834	-2.943409	0.990076
		40-120	0.899542	-3.646632	0.983955
	50	2-40	0.470384	-1.898710	0.982084
		40-120	0.911109	-3.601241	0.984341
	60	2-40	0.244205	-0.995118	0.979662
		40-120	1.333418	-5.715377	0.99152
Co	25	2-40	1.419281	-5.916515	0.999567
		40-120	0.925388	-4.319358	0.997831
	30	2-40	1.309571	-4.773036	0.998212
		40-120	0.518048	-2.316550	0.994419
	40	2-40	0.791818	-3.009265	0.975885
		40-120	1.013848	-4.016397	0.975623
	50	2-40	0.501426	-1.937673	0.979605
		40-120	1.087552	-4.211406	0.966875
	60	2-40	0.263446	-0.998486	0.981574
		40-120	1.738110	-6.697742	0.984702
Mn	25	2-40	1.259444	-5.630382	0.994598
		40-120	0.969427	-4.527444	0.998058
	30	2-40	1.151219	-4.546894	0.989801
		40-120	0.540793	-2.429524	0.995009
	40	2-40	0.828228	-3.153667	0.977150
		40-120	1.054357	-4.185792	0.975492
	50	2-40	0.531598	-2.054552	0.978774
		40-120	1.128937	-4.380284	0.964131
	60	2-40	0.268624	-1.055889	0.980419
		40-120	2.462479	-6.031695	0.989763
Fe	25	2-80	0.038950	0.360196	0.938111
	30	2-80	0.112788	0.276157	0.80763

	40	2-80	0.089662	0.320863	0.880921
	50	2-80	0.103364	0.422718	0.951322
	60	2-80	0.067914	0.665046	0.982624
Al	25	2-20	0.254812	-3.365088	0.911196
		20-120	0.789638	-5.221208	0.995633
	30	2-20	0.373905	-3.477697	0.934904
		20-120	0.629495	-4.290759	0.997092
	40	2-20	0.391407	-3.247393	0.910180
		20-120	0.846278	-4.747680	0.998395
	50	2-20	0.399550	-2.902988	0.944319
		20-120	0.828064	-4.395754	0.991437
	60	2-20	0.319569	-2.231791	0.921830
		20-120	0.969160	-4.672402	0.999891

Table S8 Ea Calculation results

Element	Fit Equation	R^2	Ea
Li	y=5.168004x+15.691994	0.969887	42.90024
Ni	y=10.499676x+30.556589	0.999198	87.21386
Co	y=11.563755x+36.859289	0.983865	96.10984
Mn	y=11.705435x+34.134966	0.979887	97.31537
Fe	y=1.787232x+6.003733	0.939136	14.79892
Al	y=5.278412x+13.550629	0.959926	43.88472

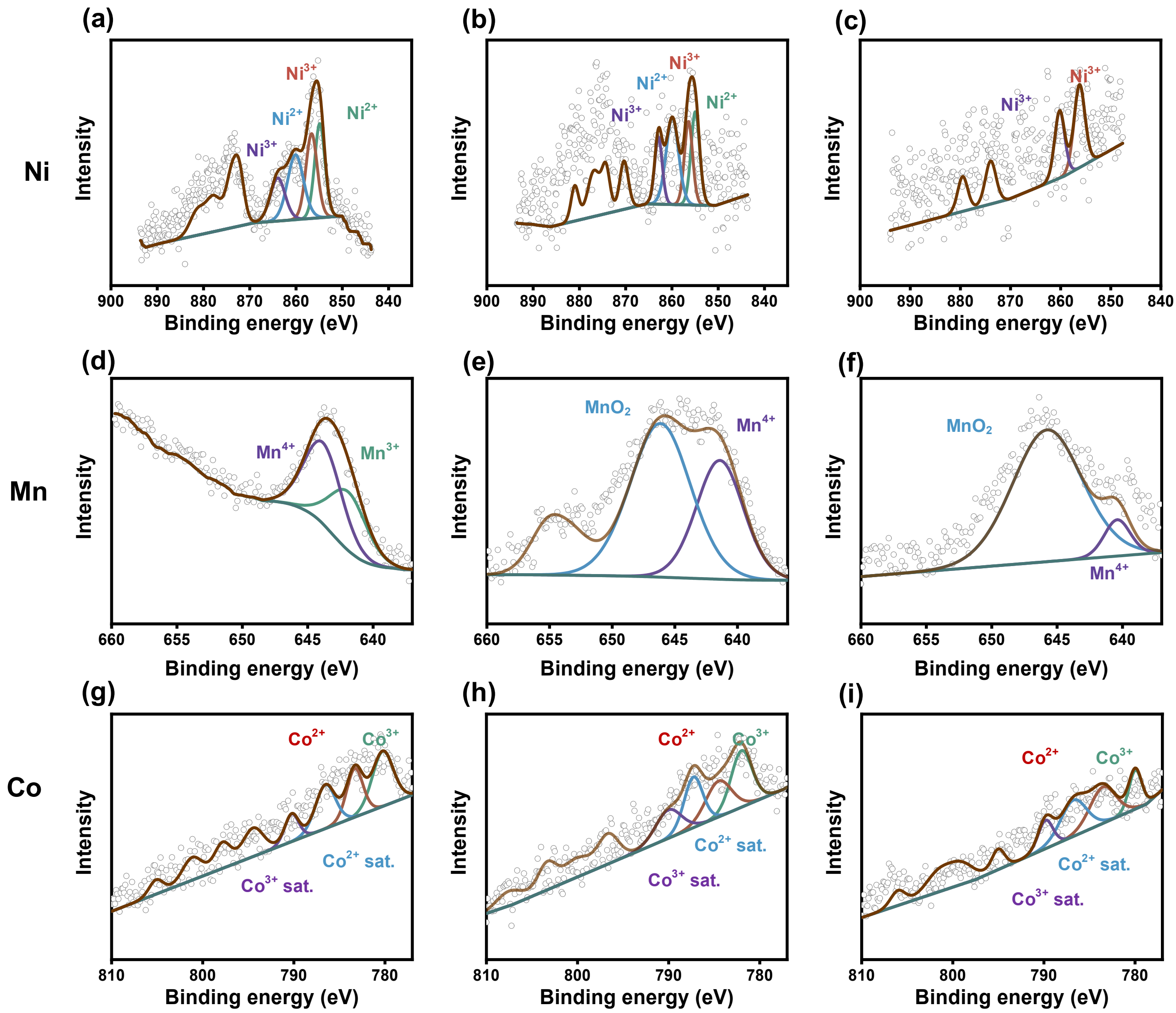

Table S13 2p3/2 Binding energies of Ni, Co, Mn for (a,d,g)positive plates of NCM, (b,e,h)NCM positive plates after leaching and (c,f,i)LFP positive plates after leaching .

Table S9 2p3/2 Binding energies of Ni, Co, Mn for different materials.

Chemical elements	Material	Binding energy $2p_{3/2}$ (eV)			
Ni	Electrode piece of NCM	854.87	856.64	860.11	863.97
	NCM after leaching	854.95	856.42	859.92	862.92
	LFP after leaching	855.75	860.125		
Co	Electrode piece of NCM	780.25	783.32	786.54	790.24
	NCM after leaching	782.01	784.53	787.28	790.03
	LFP after leaching	779.97	783.53	786.76	789.83
Mn	Electrode piece of NCM	641.89	643.83		
	NCM after leaching	641.41	646.15		
	LFP after leaching	641.12	646.12		

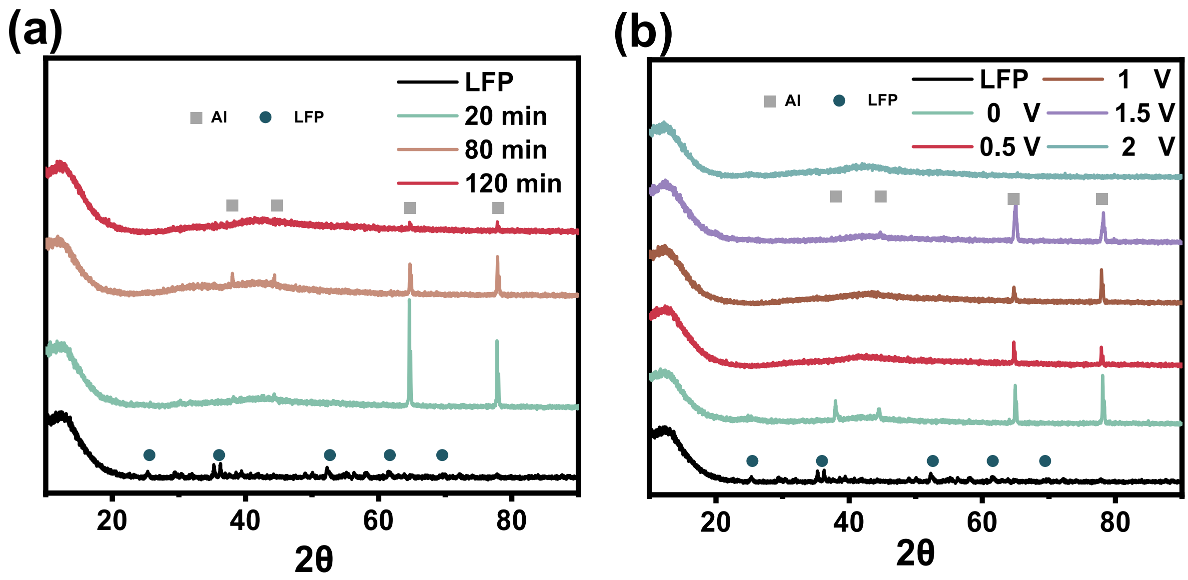

Figure S14. XRD test results of LFP electrode under (a) different leaching time and (b) different leaching voltage.

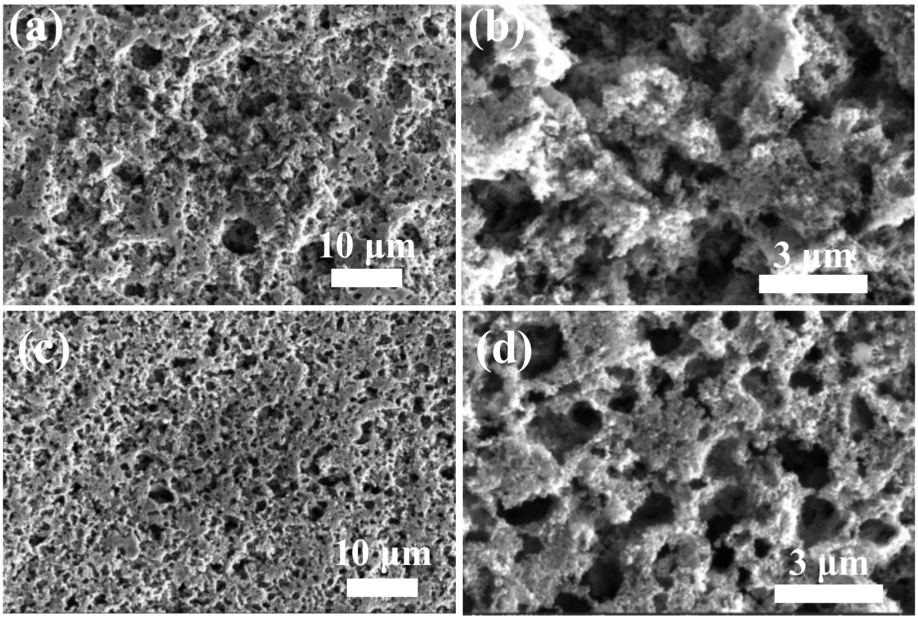

图 S15 The positive plates after leaching of LFP at (a) 0V and (b) 1V.

Finite element analysis model

The third current distribution, which is a built-in model in *COMSOL Multiphysics*, is used to predict the current density and electric potential distributions in the electrolyte. The establishment of the model is similar to *J. Colloid Interface Sci. 653 (2024) 697-706*.[1] For simplicity, the model only considers the movement of H^+, the diffusion coefficients Di of H^+ is 2E-9 m^2 s^{-1}, Um is 1E-12 s mol kg^{-1}. The concentration of the H^+ is 2 M, the current density i is 1 mA cm^{-2}, phil is 1 V. limiting diffusion current density 3 mA cm^{-2}. The electrode is porous electrode. Considering the accuracy of the simulation software system, the area inside the frame is set as Fig. S15

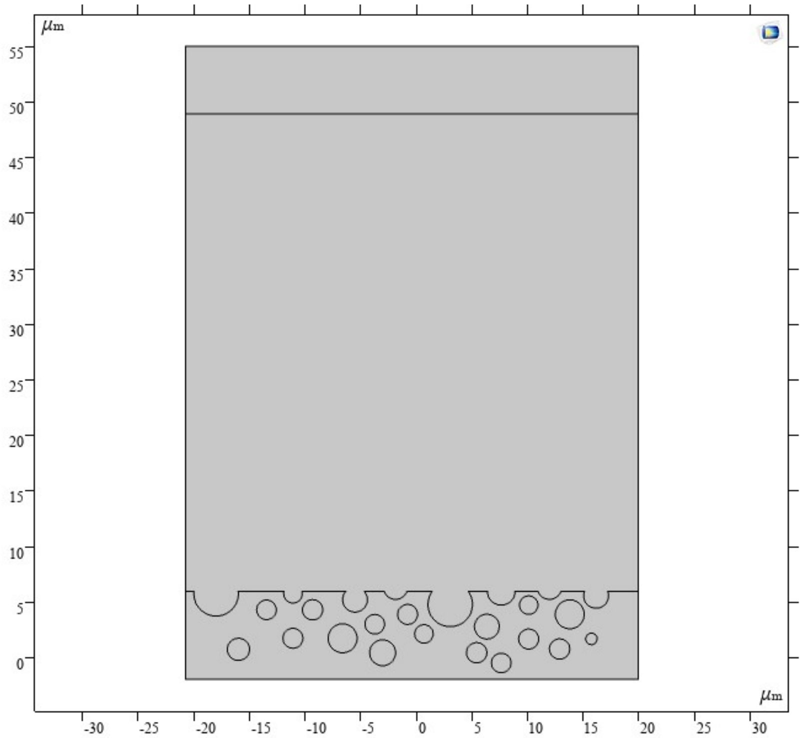

Figure S16 Geometric model

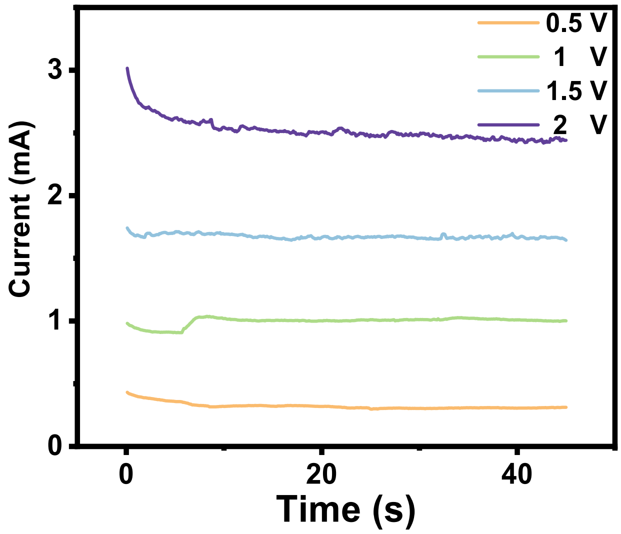

Figure S17 Results of voltage step method tests at 0.5V, 1V, 1.5V and 2V.

Pseudocapacitance calculation:
The real and imaginary components of capacitance (C' and C'', respectively) as a function of angular frequency (u) can be calculated according to Equations (S1) and (S1).

$$C'(\omega) = \frac{-Z''(\omega)}{\omega|Z(\omega)|^2} \quad \text{(S1)}$$

$$C''(\omega) = \frac{-Z'(\omega)}{\omega|Z(\omega)|^2} \quad \text{(S1)}$$

Table S10 Comparative experimental design

Group	Time (min)	Temperature (℃)	Electrolyte	Voltage (V)	Cathode	Anode
A	120	60	1M H_2SO_4	0	NCM	C
B	120	60	1M H_2SO_4	1	NCM	C
C	120	60	1M H_2SO_4 +50mg L^{-1} Fe^{3+}	1	NCM	C
D	120	60	1M H_2SO_4+50mg L^{-1} Fe^{2+}	1	NCM	C
E	120	40	1M H_2SO_4+200mg L^{-1} Fe^{2+}	1	NCM	C
F	120	40	1M H_2SO_4+200mg L^{-1} Fe^{3+}	1	NCM	C
G	60	40	1M H_2SO_4	0	C	LFP
H	60	40	1M H_2SO_4	1	C	LFP

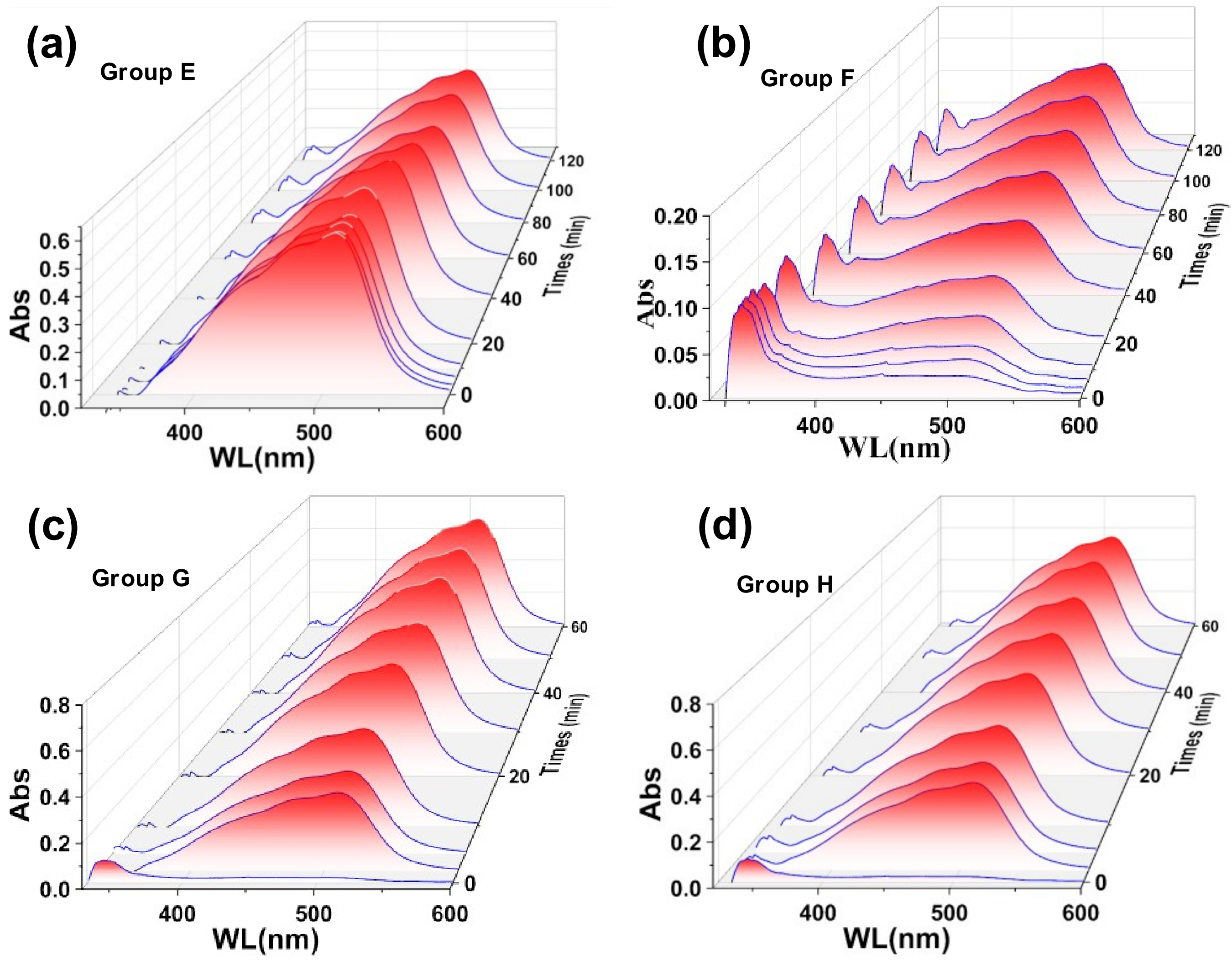

Figure S18 The complete absorbance spectra of UV-Vis results.

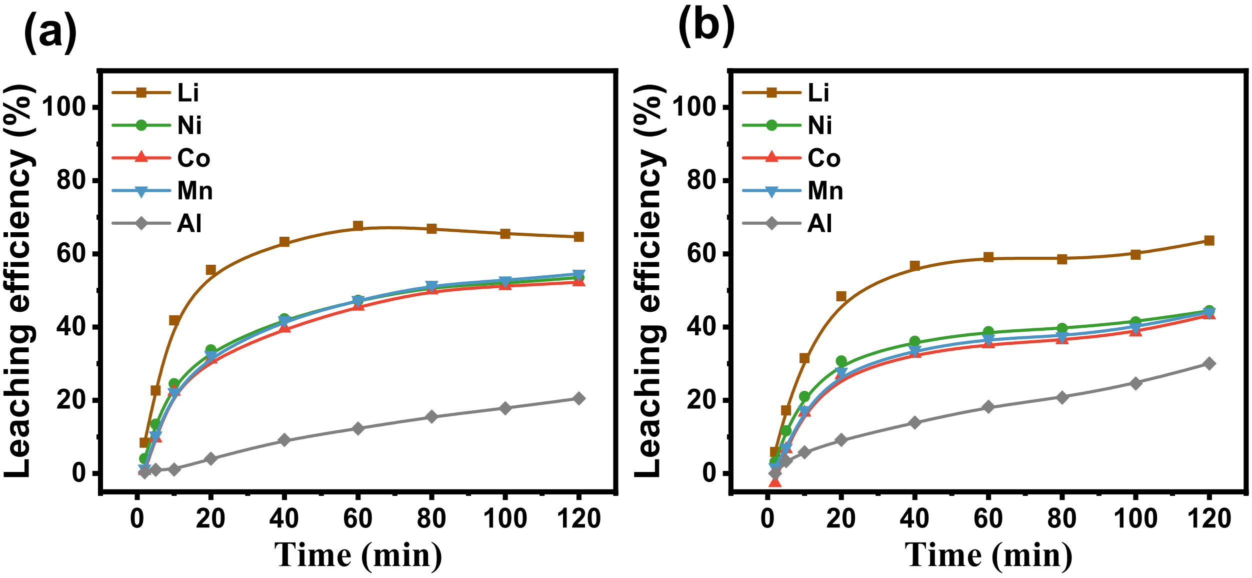

Figure S19. The leaching rate of each element in (a) group E and (b) group F at different time.

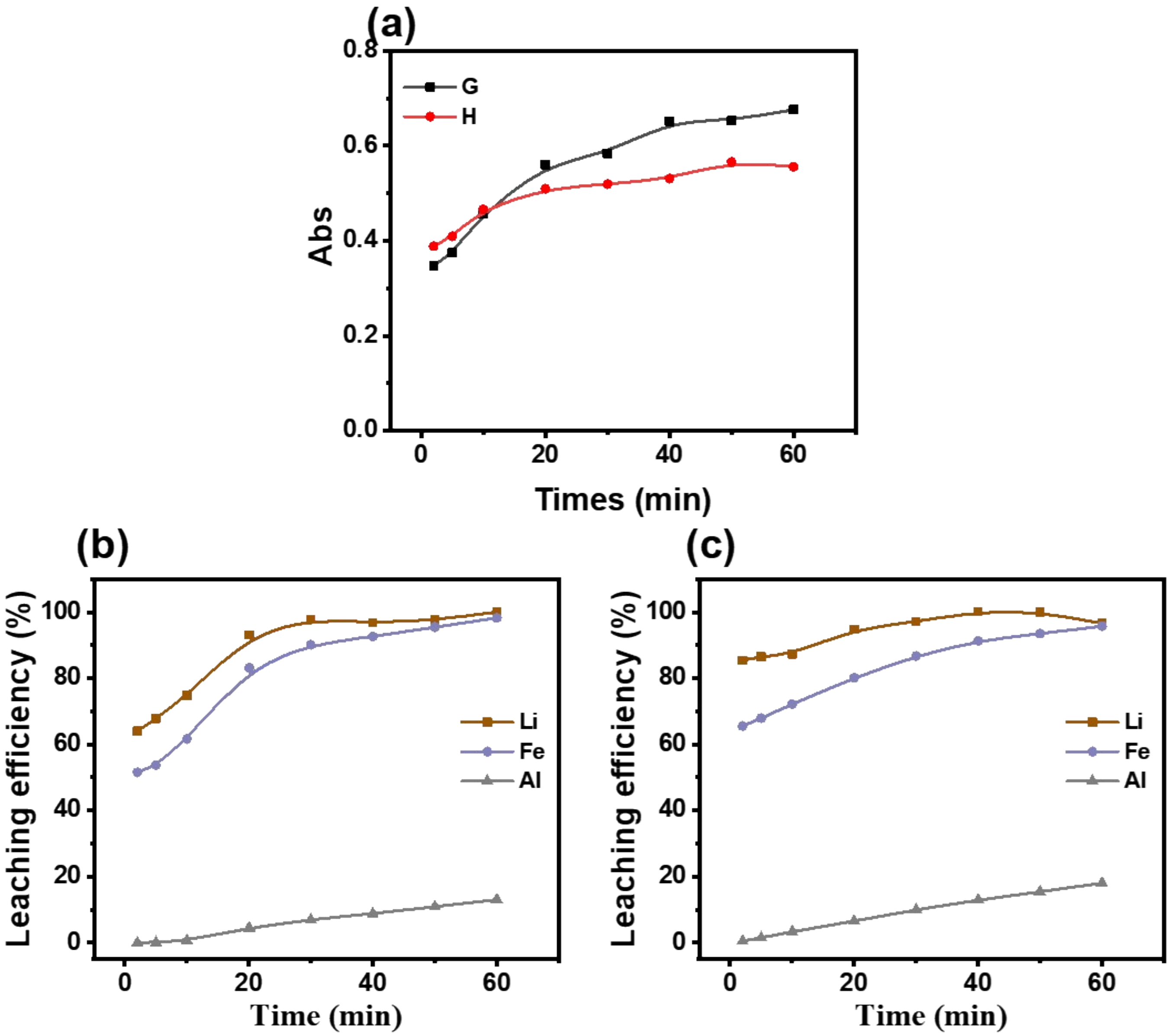

Figure S20. (a) G, H group of spectrophotometer test results, (b) G group at different times the leaching rate of each element, (c) H group at different times the leaching rate of each element.

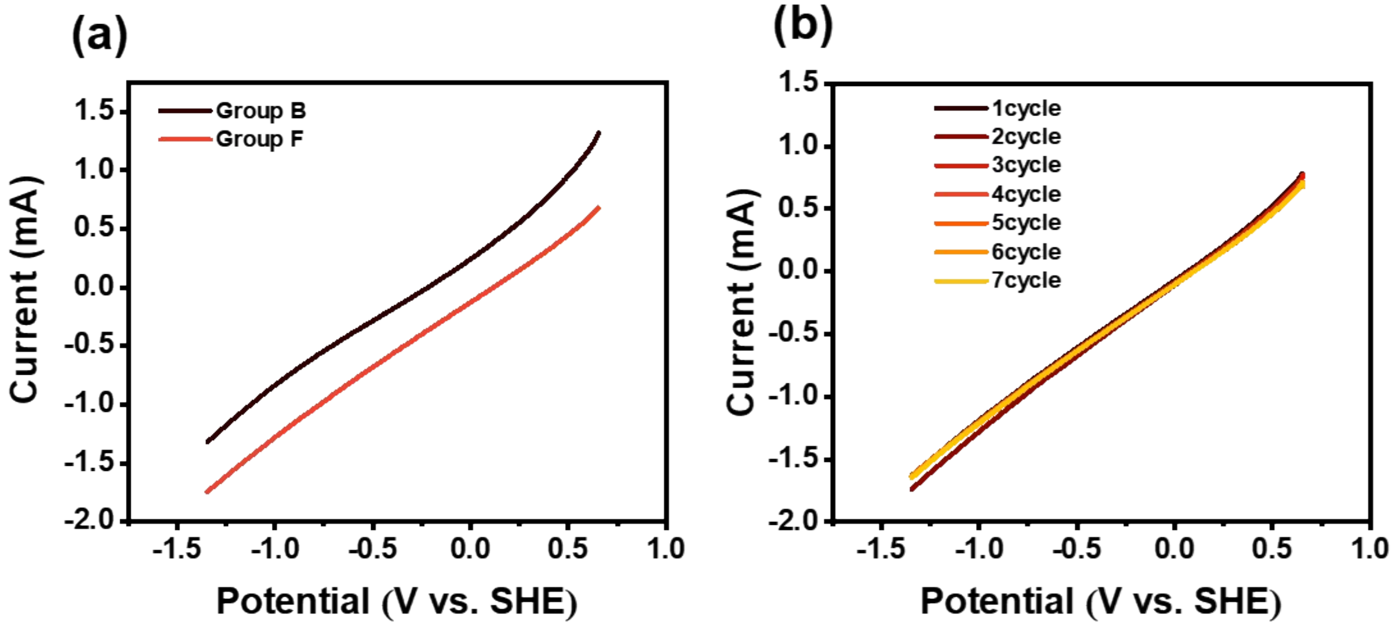

Figure S21. (a)The LSV test results of group B and group F.(b)The LSV test results of group F in different times.

Table S11 2p3/2 Binding energies of Fe different materials.

Chemical elements	Material	Binding energy $2p_{3/2}$ (eV)				
Fe	Electrode piece of LFP	712.97	710.14	716.1	725.53	
	NCM after leaching	705.99	709.16	712.76	715.64	720.03
	LFP after leaching	708.9	712.8	716.91	726.34	

Direct energy consumption of electrolysis:
Electrolytic voltage: $U =$ 1 V
Current generated by a single electrolysis: $I =$ 1 mA
Single electrolysis time: $t =$ 2 hour
The active substance dissolved by a single electrolysis: $m =$ 0.214g

energy consumption by a single electrolysis: $Q_0 = UIt = 1 \times 0.001 \times 2 = 0.002$

The energy consumption for electrolysis of M = 1 t active material: $Q = \frac{M}{m} \times Q_0 = 9.94$ kW h t[-1]

Table S12 A summary of electrochemical leaching processes for spent LIBs.

cathode	anode	Working voltage/ current	Times	electrolyte	side reaction	element	leaching efficiencies	Energy consumption of electrolysis kW h t^{-1} positive powder	Ref
LCO positive powder after calcined coating on Ti mesh	Pt	2.5 V	60 h	0.02 M H_2SO_4 +extractant	Hydrogen and Oxygen evolution	Li, Co	over 99%	≥ 1300	[2]
SS cathode	Ni	1.5-2.5 V	400 min	2 M H_2SO_4+10 mM $FeSO_4$ at membrane separated	Hydrogen and Oxygen evolution	Li, Ni, Co, Mn	over 99%	34.3	[3]
NCM powder after reductive thermal treatment	graphite	0.8 A	150 min	1.5 M H_2SO_4	Hydrogen and Oxygen evolution	Li, Ni, Co, Mn	90.59% Ni, 90.53% Co, 66.40% Mn, 100% Li	1592	[4]
spent LCO positive plate	Pt	2 V	90 min	0.5 M H_2SO_4	Hydrogen and Oxygen evolution	Li, Co	over 97 %	≥ 3000	[5]
LCO positive powder after calcined	Pt	8 V	180 min	1.25 M malic acid	Hydrogen and Oxygen evolution	Li, Co	94% Li, 90% Co	/	[6]
carbon fiber	NCM powder is coated on carbon fiber cloth	2 V	150 min	0.1 M NaCl	Hydrogen and Oxygen evolution	Li	91.37% Li	/	[7]
graphite	graphite	12 V	250 min	10% H_2SO_4+5 g/L $FeSO_4$ +LCO powder	Hydrogen and Oxygen evolution	Co	58% Co	/	[8]
spent NCM positive plate	carbon sheet	4 V	180 min	0.1 mol/L Na_2CO_3	Hydrogen and Oxygen evolution	Li	99% Li	1173	[9]

SS cathode	Pb anode	200 A m^{-2}	180 min	2 M H_2SO_4 +LCO powder	Hydrogen and Oxygen evolution	Co, Cu, Mn	96% Co, 97% Cu, 99% Mn	6500	[10]
spent NCM positive plate	Pt	32 V	5 min	2.5 g L^{-1} $(NH_4)_2SO_4$	Hydrogen and Oxygen evolution	Li	98% Li	/	[11]
Cu foil	Ti	500A m^{-2}	60 min	0.15 M $CuSO_4$	Hydrogen and Oxygen evolution, Cu electrodeposited	Li, Co	97% Li, 92% Co.	9274	[12]
spent NCM positive plate	Pt	4 V	70min	0.5 M acetic acid+ 0.05 M ascorbic acid	Hydrogen and Oxygen evolution	Li, Ni, Co, Mn	over 99%	/	[13]
spent LCO positive plate	Pt	8V	120 min	2.5 M DL-malic acid	Hydrogen and Oxygen evolution	Li, Co	98.12 % Li, 97.36 % Co	/	[14]
spent NCM positive plate	spent LFP positive plate	1V	120 min	1 M H_2SO_4	without side reaction	Li, Ni, Co, Mn, Fe	over 99%	9.94	This work

Reference

[1.]Zhong, K.; Hou, X.; Xue, Y.; Huang, W.; Meng, B.; Zhou, L.; Fang, Z.; Li, L., Lithium metal deposition under the geometrical confinement effect: Dendritic copper foam current collector. *J. Colloid Interface Sci.* **2024,** *653*, 697-706.
[2.]Zhao, J.; Zhou, F.; Wang, H.; Qu, X.; Wang, D.; Cai, Y.; Zheng, Z.; Wang, D.; Yin, H., Coupling Electrochemical Leaching with Solvent Extraction for Recycling Spent Lithium-Ion Batteries. *Environ. Sci. Technol.* **2024,** *58*, (38), 16803-16814.
[3.]Diaz, L. A.; Strauss, M. L.; Adhikari, B.; Klaehn, J. R.; McNally, J. S.; Lister, T. E., Electrochemical-assisted leaching of active materials from lithium ion batteries. *Resources, Conservation and Recycling* **2020,** *161*, 104900.
[4.]Lei, S.; Zhang, Y.; Song, S.; Xu, R.; Sun, W.; Xu, S.; Yang, Y., Strengthening Valuable Metal Recovery from Spent Lithium-Ion Batteries by Environmentally Friendly Reductive Thermal Treatment and Electrochemical Leaching. *ACS Sustain. Chem. Eng.* **2021,** *9*, (20), 7053-7062.
[5.]Zhao, J. J.; Qu, J. K.; Qu, X.; Gao, S. B.; Wang, D. H.; Yin, H. Y., Cathode electrolysis for the comprehensive recycling of spent lithium-ion batteries. *Green Chem.* **2022,** *24*, (16), 6179-6188.
[6.]Meng, Q.; Zhang, Y.; Dong, P., Use of electrochemical cathode-reduction method for leaching of cobalt from spent lithium-ion batteries. *J. Clean. Prod.* **2018,** *180*, 64-70.
[7.]Lv, H.; Huang, H.; Huang, C.; Gao, Q.; Yang, Z.; Zhang, W., Electric field driven de-lithiation: A strategy towards comprehensive and efficient recycling of electrode materials from spent lithium ion batteries. *Applied Catalysis B: Environmental* **2021,** *283*, 119634.
[8.]Zeng, G.; Luo, S.; Li, H.; Wang, X., Innovative Electrochemistry Technique for Leaching Cobalt from Spent Lithium Ion Batteries. *Asian J. Chem.* **2014,** *26*, (4), 1099.
[9.]Dang, S.; Hou, W.; Min, Y.; Wu, J.; Xu, Q.; Shi, P., Electro-oxidation: A win–win strategy for the selective recovery of Li+ from spent lithium-ion batteries and the preparation of highly active catalysts. *Chem. Eng. J.* **2022,** *435*, 135169.
[10.]Prabaharan, G.; Barik, S.; Kumar, N.; Kumar, L., Electrochemical process for electrode material of spent lithium ion batteries. *Waste Manag.* **2017,** *68*, 527-533.
[11.]Liu, K.; Yang, S.; Lai, F.; Wang, H.; Huang, Y.; Zheng, F.; Wang, S.; Zhang, X.; Li, Q., Innovative electrochemical strategy to recovery of cathode and efficient lithium leaching from spent lithium-ion batteries. *ACS Appl. Energy Mater.* **2020,** *3*, (5), 4767-4776.
[12.]Li, S.; Wu, X.; Jiang, Y.; Zhou, T.; Zhao, Y.; Chen, X., Novel electrochemically driven and internal circulation process for valuable metals recycling from spent lithium-ion batteries. *Waste Manag.* **2021,** *136*, 18-27.
[13.]Yang, K.; Zhu, C.; Li, J.; Meng, B.; Zhong, K.; Huang, W.; Yu, J.; Fang, Z., Electric field-assisted leaching of valuable metals from spent lithium-ion batteries in a mixture of acetic acid and ascorbic acid. *Hydrometallurgy* **2023,** *221*, 106152.
[14.]Zhou, S.; Zhang, Y.; Meng, Q.; Dong, P.; Yang, X.; Liu, P.; Li, Q.; Fei, Z., Recycling of spent LiCoO2 materials by electrolytic leaching of cathode electrode plate. *J. Environ. Chem. Eng.* **2021,** *9*, (1), 104789.